

# Majindeite, $\text{Mg}_2\text{Mo}_3\text{O}_8$ , a new mineral from the Allende meteorite and a witness to post-crystallization oxidation of a Ca-Al-rich refractory inclusion

CHI MA<sup>1,\*</sup> AND JOHN R. BECKETT<sup>1</sup>

<sup>1</sup>Division of Geological and Planetary Sciences, California Institute of Technology, Pasadena, California 91125, U.S.A.

## ABSTRACT

Majindeite (IMA 2012-079),  $\text{Mg}_2\text{Mo}_3\text{O}_8$ , is a new mineral, occurring as submicrometer-sized crystals with Ni-Fe and Ru-Os-Ir alloys,  $\pm$  apatite and Nb-oxide. The observed assemblages are partially or wholly enclosed by  $\text{MgAl}_2\text{O}_4$  spinel in a Type B1 Ca-Al-rich inclusion, *ACM-2*, from the Allende CV3 carbonaceous chondrite. The type majindeite has an empirical formula of  $(\text{Mg}_{1.57}\text{Fe}_{0.43})\text{Mo}_{3.00}\text{O}_8$ , and a nolanite-type *P6<sub>3</sub>mc* structure with  $a = 5.778 \text{ \AA}$ ,  $c = 9.904 \text{ \AA}$ ,  $V = 286.35 \text{ \AA}^3$ , and  $Z = 2$ , leading to a calculated density of  $5.54 \text{ g/cm}^3$ .

Majindeite likely formed during the subsolidus oxidation of Mo-rich precursor phase(s) included in Fe-Ni rich alloys in a system that was open to O, Mg, and Ca, which were derived externally and introduced via cracks, subgrain boundaries, and/or surfaces exposed at the exterior of the spinel. If magnetite existed in the phase assemblage, it was lost due to Fe volatilization prior to the formation of majindeite. The immediate precursor to majindeite was likely kamiokite. Majindeite formed during an oxidation event contemporaneous with or postdating the formation of grossular-rich veins in melilite.

Kamiokite, the Fe-rich analog of majindeite, also occurs in *ACM-2* but only within phase assemblages that contain magnetite and which are entirely enclosed in melilite  $\pm$  alteration products. Here, grossular-rich veins are not observed and the coexisting awaruites are more Fe-rich than those observed with majindeite. As with majindeite, the precursors for kamiokite grains were also likely to have been Mo-rich alloys, but the Mo-oxide remained magnetite-saturated throughout the alteration process and therefore remained Fe-rich.

**Keywords:** Majindeite,  $\text{Mg}_2\text{Mo}_3\text{O}_8$ , new mineral, kamiokite group, Allende meteorite, CV3 carbonaceous chondrite, EBSD, Ca-Al-rich inclusions

## INTRODUCTION

The origin and evolution of Ca-Al-rich inclusions (CAIs) in meteorites is a story of the origin and early evolution of the Solar System. Although bulk compositions of these objects can aid in deciphering some of the pages (e.g., Beckett and Grossman 1988; Grossman et al. 2000), it is in the constituent minerals that most of the information on environment lies. New minerals can provide special insight because they sample special environments not encountered by most inclusions (e.g., Ma et al. 2011b) or because they represent responses to aspects of an environment that was encountered by other phases but poorly recorded (e.g., Ma et al. 2014a). In this work, we consider a new Mo-Mg oxide mineral, majindeite,  $\text{Mg}_2\text{Mo}_3\text{O}_8$ , which was discovered in the Allende Type B1 Ca-Al-rich inclusion (CAI) *ACM-2*. In addition to majindeite, this inclusion is the source of three previously described new minerals, grossmanite ( $\text{CaTi}^{3+}\text{AlSiO}_6$ ), monipite ( $\text{MoNiP}$ ), and nuwaite ( $\text{Ni}_6\text{GeS}_2$ ) (Ma and Rossman 2009b; Ma et al. 2014a; Ma 2015a), and two first occurrences in a meteorite for the Mo-oxides tugarinovite ( $\text{MoO}_2$ ) and kamiokite ( $\text{Fe}_2\text{Mo}_3\text{O}_8$ ) (Ma et al. 2014a). Molybdenum is a major constituent of five different minerals in this inclusion [majindeite, kamiokite, monipite, tugarinovite, and molybdenite ( $\text{MoS}_2$ )], which speaks

to varying fates for Mo that depend on microenvironment and initial phase composition tied together through a common thread of thermal and metasomatic processing.

Phases of the type  $\text{X}_2\text{Mo}_3\text{O}_8$ , where X is a divalent cation, are readily synthesized using a wide variety of cations including Cd, Co, Cu, Fe, Mg, Mn, Ni, and Zn (e.g., McCarroll et al. 1957; Knorr and Mueller 1995; Abe et al. 2010) and they are of considerable interest in research on frustrated magnetic systems (e.g., Nakayama et al. 2011) because of the layered honeycomb structures in which Mo-O and  $\text{X}^{2+}$ -O coordinated sheets alternate. However, only two of these compounds, kamiokite ( $\text{Fe}_2\text{Mo}_3\text{O}_8$ ) and iseite ( $\text{Mn}_2\text{Mo}_3\text{O}_8$ ), were previously known to exist in nature (e.g., Johan and Picot 1986; Nishio-Hamane et al. 2013). In this work, we describe the first occurrence in nature of the Mg-end-member of the  $\text{X}_2\text{Mo}_3\text{O}_8$  class of phases. This mineral is named majindeite ( $\text{Mg}_2\text{Mo}_3\text{O}_8$ ). We show through electron backscatter diffraction (EBSD) that majindeite has a nolanite-type *P6<sub>3</sub>mc* structure, isostructural with kamiokite and iseite. We use electron probe microanalysis (EPMA) and high-resolution scanning electron microscopy (SEM) to characterize the petrographic settings and compositions of majindeite and associated phases. We then connect these data and those for kamiokite-bearing phase assemblages, which also occur in the CAI *ACM-2*, to implications for precursors and the processes that led to their formation. Preliminary results of this work are given by Ma et al. (2009).

\* E-mail: chi@gps.caltech.edu

### MINERAL NAME AND TYPE MATERIAL

The mineral and the mineral name (majindeite) have been approved by the Commission on New Minerals, Nomenclature and Classification (CNMNC) of the International Mineralogical Association (IMA 2012-079) (Ma 2013). The name is in honor of Ma Jinde (1939–1991), a mineralogist at the China University of Geosciences (Wuhan), China, who passed away during a teaching field trip. He demonstrated in his classes and in the field that mineralogy can be great fun and introduced SEM and EPMA techniques to the first author. Ma Jinde contributed to mineralogical investigations of many mines and regions in China, including the Baiyun Obo rare earth element-iron mine in the 1960s, where he was the lead mineralogist in charge of mineral separation.

The holotype material for majindeite occurs within a Caltech optically thick polished section of Allende (Allende 12, section E) in the type B1 CAI *ACM-2*, which is deposited under catalog no. USNM 7615 in the Smithsonian Institution's National Museum of Natural History, Washington, D.C. Holotype materials for two recently described new minerals, grossmanite and monipite, occur in a different section (USNM 7554) obtained from the same CAI (Ma and Rossman 2009b; Ma et al. 2014a).

### OCCURRENCE

The Allende meteorite fell in and near Pueblito de Allende, Chihuahua, Mexico, on February 8, 1969 (Clarke et al. 1971). This CV3 carbonaceous chondrite is probably the most heavily studied meteorite in existence and the results of these studies have greatly influenced current thinking about processes, timing, and chemistry in the primitive solar nebula and in small planetary bodies. Allende continues to be a source of new information on materials produced in the early Solar System. For example, majindeite is just 1 of 16 new minerals discovered in Allende since 2007 (Ma 2015b; Ma et al. 2015).

The mineral majindeite is present within the CAI, *ACM-2*, which was serially sectioned from a ~1 cm diameter Allende fragment (Caltech Meteorite Collection No. Allende12A). Only a small portion of a once much larger inclusion, bounded by a matrix of mostly fine-grained olivine and troilite, still exists, and this leads to ambiguity concerning the nature of the host inclusion. Ma et al. (2014a) argued, based primarily on geometric considerations and the presence of low-Ti clinopyroxene phenocrysts, that *ACM-2* was a large type B1 CAI, ~7 mm in diameter, and that the presence of a Wark-Lovering rim where the inclusion contacts matrix implies that the remaining material was originally a portion of the melilite-rich mantle. We accept this designation in the present work and refer the reader to Ma and Rossman (2009b) and Ma et al. (2014a) for additional mineral compositions and a general petrographic description of this inclusion.

Figure 1a shows a backscattered electron (BSE) image of the region containing the holotype material in USNM 7615 and the location of the majindeite, which is ~600  $\mu\text{m}$  from the rim of *ACM-2*. Figure 1b shows a close-up of the majindeite-bearing phase assemblage in host spinel and melilite (Ak24). Two subhedral majindeite grains,  $0.5 \times 1.0 \mu\text{m}$  and  $0.15 \times 0.3 \mu\text{m}$ , and euhedral majindeite nanolaths, occur in a  $3 \times 4 \mu\text{m}$  phase assemblage, which is mostly enclosed by spinel

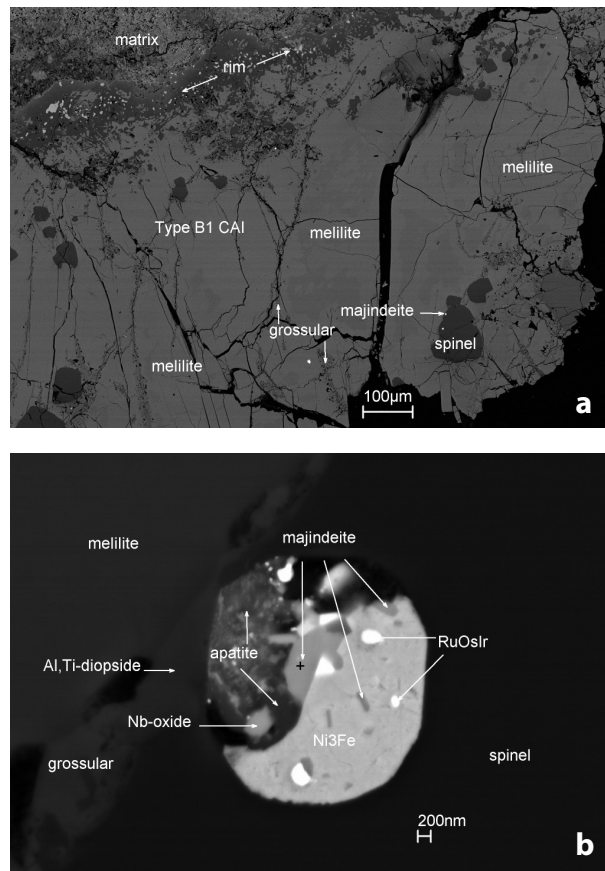


**FIGURE 1.** (a) Backscattered electron (BSE) image showing part of the Type B1 CAI *ACM-2* in USNM 7615. (b) Enlarged BSE image revealing majindeite with apatite, Nb-oxide, Ni-Fe, and Ru-Os-Ir alloys within a spinel grain in host melilite. The type majindeite crystal is marked with a cross. The tiny gray laths in Fe-Ni alloy are all majindeite.

[ $\text{Mg}_{1.00}(\text{Al}_{1.97}\text{Ti}_{0.01}\text{V}_{0.01}\text{Cr}_{0.01})\text{O}_4$ ; containing <0.3 wt% FeO] but also bordered in part by a thin bleb of Al-,Ti-rich diopside [ $(\text{Ca}_{0.79}\text{Mg}_{0.60}\text{Al}_{0.36}\text{Ti}_{0.25})(\text{Si}_{1.16}\text{Al}_{0.84})\text{O}_6$ ]. A solid solution of clinopyroxene, ranging in composition from Al-,Ti-rich diopside to grossmanite, is commonly observed in contact with spinels in *ACM-2* and other type B1 inclusions (e.g., Paque et al. 2009). The Al-,Ti-rich diopside is bounded by a grossular-rich vein after melilite. Within the majindeite-bearing phase assemblage, apatite is in contact with the Al-,Ti-rich diopside, awaruite ( $\text{Ni}_{74}\text{Fe}_{25}\text{Pt}_2$ ), which contains inclusions of Ru-Os-Ir alloys (Ru/Os/Ir atomic ratio: ~63:32:5) and Mo-bearing oxides (elongate crystals in Fig. 1b), and spinel. There is also a grain of Nb-rich oxide within the apatite, which is likely a new mineral but too small for a full investigation using currently available techniques. Both of the majindeite grains are in contact with awaruite, the largest of which is roughly centered in the phase assemblage and contacts apatite, awaruite, and Ru-Os-Ir alloy grains.

An additional grain of majindeite, ~1.0  $\mu\text{m}$  wide, was observed in a  $3 \times 5 \mu\text{m}$  inclusion within *ACM-2* in Caltech sample Allende 12, section B2 (Fig. 2). This inclusion is dominated by a single crystal of awaruite ( $\text{Ni}_{82}\text{Fe}_{15}\text{Pt}_2\text{Rh}_1$ ), labeled “NiFe” in Figure 2b, wholly enclosed in spinel [ $(\text{Mg}_{0.93}\text{Fe}_{0.04}\text{Ca}_{0.01})(\text{Al}_{1.99}\text{Ti}_{0.01}\text{V}_{0.01})\text{O}_4$ ,

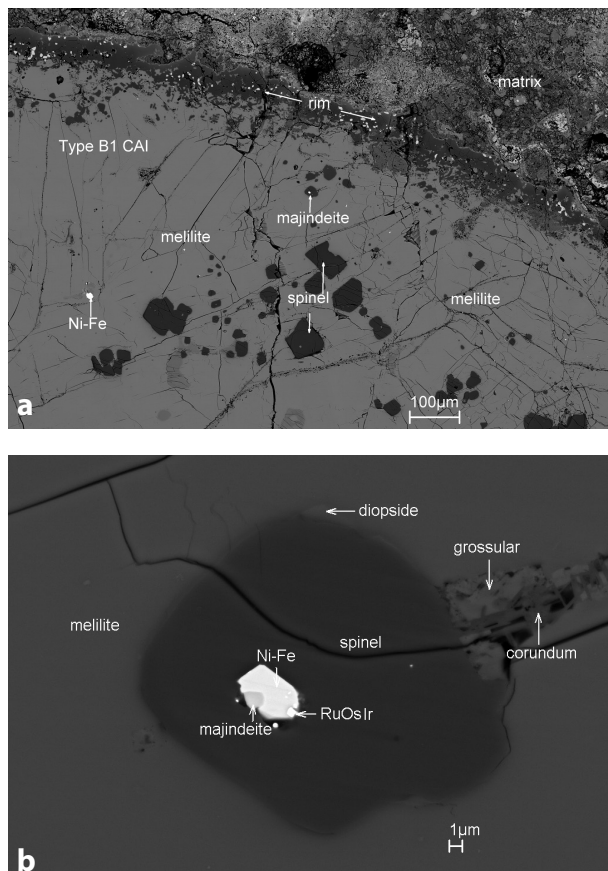


**FIGURE 2.** (a) BSE image showing a second occurrence of majindeite in *ACM-2* (Caltech section Allende 12, section B2). (b) Enlarged BSE image revealing that this majindeite-bearing phase assemblage is completely enclosed by spinel, which is mostly enclosed by melilite (Ak11). An alteration vein composed of grossular plus a highly aluminous phase (corundum?) intersects the spinel on one side and there are also some small blebs of grossmanite (boundary clinopyroxenes in the parlance of Paque et al. 2009).

with 2.1 wt% FeO) that contains grains of Ru-Os-Ir alloy (Ru/Os/Ir/Mo atomic ratio:  $\sim 57:15:3:1$ ), although not in contact with the majindeite. Most of the majindeite grain contacts the Ni-rich alloy; some is in contact with spinel and material along one side near spinel is missing (Fig. 2b). The spinel host of this majindeite crystal is only  $\sim 140 \mu\text{m}$  from the rim of the inclusion. Note that a vein containing grossular plus a highly aluminous phase (corundum?) is in contact with one side of the host spinel. Given that sections through *ACM-2* are roughly perpendicular to the surface of the inclusion (Ma et al. 2014a), the much greater distance to the inclusion rim for the majindeite shown in Figure 1 implies that the occurrence of majindeite is not strongly dependent on distance from the rim. There is, however, a petrographic commonality for both majindeite occurrences in their association with spinel and grossular-rich veins. The kamiokite-bearing phase assemblages are also variably distributed within the mantle of *ACM-2* (e.g., Fig. 5 of Ma et al. 2014a) and they too have a petrographic commonality in that all of the other Mo-rich phases observed in *ACM-2* are in phase assemblages included within melilite [five

occurrences of kamiokite ( $\text{Fe}_2\text{Mo}_3\text{O}_8$ ); one occurrence each of tugarinovite ( $\text{MoO}_2$ ) and monipite ( $\text{MoNiP}$ ), both of which occur in a kamiokite-bearing phase assemblage (see Ma et al. 2014a); one occurrence of molybdenite ( $\text{MoS}_2$ )]; none of these is associated with a grossular-rich vein. Thus, phase assemblages containing majindeites are at least partially enclosed by spinel associated with grossular-rich veins and all other Mo-rich phases, including kamiokites, are invariably included in melilite.

Both of the majindeite-bearing phase assemblages are truncated by faces with spinel that intersect at high angles (Figs. 1b and 2b) and are consistent with zones containing interfacial angles of 60, 90, and 120°, suggestive of a hexagonal or cubic (in certain orientations) crystal. These angles may refer to the outline of a precursor crystal included in spinel (e.g., a  $P6_3/mmc$  alloy such as hexamolybdenum) or a negative crystal imposed by the host spinel. The latter requires that both of the majindeite occurrences sample a plane roughly perpendicular to a  $[111]$  axis of the spinel. Because the observed axes perpendicular to the plane of the section are  $[103]$  for the spinel host of the type majindeite shown in Figure 1b (there is also a fine-grained inclusion within the spinel host for the type example that has a trigonal outline) and  $[156]$  for the host spinel grain in section B2 (Fig. 2b), the crystallographic observations are consistent with negative crystals. The fact that the phase assemblage for both majindeite occurrences display outlines independent of the phases within the assemblage suggests that the current multiphase assemblages shown in Figures 1 to 2 are pseudomorphs.

#### APPEARANCE, PHYSICAL AND OPTICAL PROPERTIES

Majindeite was observed as three small subhedral grains in *ACM-2*, two grains that were  $\sim 0.5 \times 1$  and  $0.15 \times 0.30 \mu\text{m}$  in the section plane of USNM 7615 (Fig. 1), and one  $\sim 1 \mu\text{m}$  grain in Caltech Allende 12 section B2 (Fig. 2). The larger grain (marked with a cross) in Figure 1b is the type material. The  $\sim 1 \mu\text{m}$  majindeite crystal shown in Figure 2b unfortunately plucked during a polishing touchup and was lost.

Color, luster, streak, hardness, tenacity, cleavage, fracture, density, and optical properties could not be determined experimentally because of the small grain size, but these properties may be similar to those of kamiokite. The density, calculated from its crystal structure and the empirical formula, as described below, is  $5.54 \text{ g/cm}^3$  using the cell parameters of Knorr and Mueller (1995). As might be expected based on the relative atomic weights of Mg, Fe, and Mn, this is similar to but lower than densities of the other known  $\text{X}_2\text{Mo}_3\text{O}_8$  minerals, kamiokite ( $5.79 \text{ g/cm}^3$ ; Johan and Picot 1986) and iseite ( $5.84 \text{ g/cm}^3$ ; Nishio-Hamane et al. 2013). Majindeite is not cathodoluminescent under the electron beam, and we observed no crystal forms or twinning.

#### CHEMICAL COMPOSITION

Chemical analyses of majindeite and associated spinel and melilite were carried out using a JEOL 8200 electron microprobe interfaced with the Probe for EPMA program from Probe Software, Inc., and operated in focused beam mode at 10 kV and 5 nA to minimize the interaction volume on majindeite (estimated to be  $\sim 500 \text{ nm}$  in diameter using Monte Carlo simulations through the electron trajectory program Casino v2.42), and 15 kV and 20 nA for spinel and melilite. Standards for the analysis of majindeite



and other oxides were Mo metal ( $MoL\alpha$ ), MgO ( $MgK\alpha$ ), fayalite ( $FeK\alpha$ ), spinel ( $AlK\alpha$ ), NiO ( $NiK\alpha$ ), anorthite ( $SiK\alpha$ ,  $CaK\alpha$ ), albite ( $NaK\alpha$ ),  $TiO_2$  ( $TiK\alpha$ ),  $Cr_2O_3$  ( $CrK\alpha$ ), and  $V_2O_5$  ( $VK\alpha$ ). Quantitative elemental microanalyses were processed with the CITZAF correction procedure (Armstrong 1995) and analytical results are given in Tables 1 (majindeite) and 2 (associated oxides). An Oxford INCA X-ray energy-dispersive spectrometer (EDS) on a ZEISS 1550VP field emission SEM was also used for elemental analysis of associated alloys. These data were processed using the XPP correction procedure of Pouchou and Pichoir (1991) and Oxford factory internal standards. Ma and Rossman (2009b) and Ma et al. (2014a) give compositions of the major igneous phases in *ACM-2* and of various phases associated with kamiokite in one occurrence.

The end-member formula for majindeite is  $Mg_2Mo_3O_8$ , which gives 17.36 wt% MgO and 82.64 wt%  $MoO_2$ , referenced to an oxide sum of 100. The type majindeite (section USNM 7615; Fig. 1b) has an empirical formula of  $(Mg_{1.57}Fe_{0.43})Mo_{3.00}O_8$ , which is very similar to the composition of the majindeite grain in Figure 2b (section B2),  $(Mg_{1.66}Fe_{0.36})Mo_{2.99}O_8$ . Figure 3 shows a histogram of Mg# values [molar  $Mg/(Mg+Fe)$  expressed as percent] for majindeite and kamiokite from *ACM-2*. The oxide compositions hint at two distinct populations (melilite-hosted and spinel-hosted), rather than a continuum. This contrasts with the observation of Ma et al. (2014b) for hexamolybdenum and

other refractory element-rich alloys. Given that both minerals occur in the same CAI, this suggests that the observed differences in composition reflect fundamental differences in petrogenesis. Magnesium contents were not determined for the terrestrial kamiokites and iseites (e.g., Sasaki et al. 1985; Johan and Picot 1986; Nishio-Hamane et al. 2013). However, good oxide sums and stoichiometry for most of the reported analyses would suggest that the actual Mg# values are, at the least, significantly lower than in the Allende *ACM-2* kamiokites and far lower than in majindeite.

### COEXISTING PHASES

All of the Mo-oxides in *ACM-2* are parts of multi-phase assemblages and those containing majindeite are hosted by spinel. In this section, we first describe the host spinels and then focus on the included phase assemblages. Although we emphasize majindeite, we also consider kamiokite-bearing phase assemblages, especially where there are contrasting observations, because these provide additional clues to the origin of all Mo-rich oxides in *ACM-2*.

Iron contents of the two majindeite-hosting spinels differ by an order of magnitude. In *ACM-2*, the spinels closest to the Wark-Lovering rim are considerably more FeO-rich than those in the interior. The host spinel shown in section B2 (Fig. 2b) is close to the rim (Fig. 2a) and has ~2 wt% FeO. The host spinel shown in Figure 1b (section USNM 7615) is much further away and has ~0.2 wt% FeO. The general decrease of Fe content in spinel with distance from the rim and proximity to alteration products is commonly observed in Allende CAIs and is generally thought to reflect late-stage metasomatism (e.g., Krot et al. 1995). The order of magnitude difference in Fe concentrations in host spinel for occurrences of majindeite with essentially the same composi-

**TABLE 1.** EPMA data for majindeite

Constituent	Type majindeite		
	Raw <sup>a</sup> (n = 4 <sup>b</sup> )	Processed <sup>c</sup>	Normalized
MoO <sub>2</sub>	60(1) <sup>c</sup>	60.0	80.3
MgO	10.4(0.2)	9.9	13.3
FeO	5.01(0.09)	4.8	6.4
Al <sub>2</sub> O <sub>3</sub>	1.2(0.3)		
NiO	0.7(0.2)		
Total	77.6 <sup>d</sup>	74.7	100.0

<sup>a</sup> These are raw data where Al is from the host spinel, and Ni is from adjacent Ni-Fe alloy.

<sup>b</sup> n = number of analyses.

<sup>c</sup> Errors given inside parentheses are one standard deviation of the mean based on all of the analyses.

<sup>d</sup> The low total is due to the small grain size. Missing elements are Ru, Os, Ir, Ca, P, and associated O, from adjacent Ru-Os-Ir alloy and apatite, revealed by EDS analysis but not analyzed by EPMA to avoid unwanted matrix corrections.

<sup>e</sup> Processed result of raw data via removal of Al and associated Mg from spinel  $[Mg_{1.00}(Al_{1.97}Ti_{0.01}Cr_{0.01}V_{0.01})O_4]$  and Ni plus associated Fe from Ni-Fe alloy  $(Ni_{0.739}Fe_{0.245}Pt_{0.016})$ .

**TABLE 2.** EPMA data for associated spinel and melilite

Constituent	Spinel hosting	Melilite near	Spinel hosting	Melilite near
	type majindeite	type majindeite	type majindeite	type majindeite
	in Fig. 1	in Fig. 1	in Fig. 2	in Fig. 2
wt%	n = 6 <sup>a</sup>	n = 7	n = 10	n = 12
SiO <sub>2</sub>	0.06(0.01) <sup>b</sup>	26.2(0.5)	0.03(0.01)	24.4(0.3)
Al <sub>2</sub> O <sub>3</sub>	70.1(0.6)	26.3(0.6)	70.4(0.2)	31.4(0.4)
MgO	28.0(0.8)	4.5(0.3)	25.9(0.6)	1.8(0.2)
CaO	0.08(0.03)	43.0(0.5)	0.24(0.02)	41.7(0.4)
Na <sub>2</sub> O	b.d. <sup>c</sup>	0.05(0.04)	b.d.	b.d.
V <sub>2</sub> O <sub>5</sub>	0.49(0.01)	b.d.	0.75(0.02)	b.d.
TiO <sub>2</sub>	0.36(0.02)	0.05(0.03)	0.39(0.02)	b.d.
Cr <sub>2</sub> O <sub>3</sub>	0.33(0.03)	0.06(0.02)	0.12(0.03)	b.d.
FeO	b.d.	b.d.	2.1(0.3)	b.d.
Total	99.4	100.2	99.9	99.3

<sup>a</sup> n = number of analyses.

<sup>b</sup> Errors given inside parentheses are one standard deviation of the mean based on all of the analyses.

<sup>c</sup> b.d. = below detection limit, Na 0.02 wt%, V 0.02 wt%, Ti 0.04 wt%, Cr 0.05 wt%, Fe 0.3 wt%.

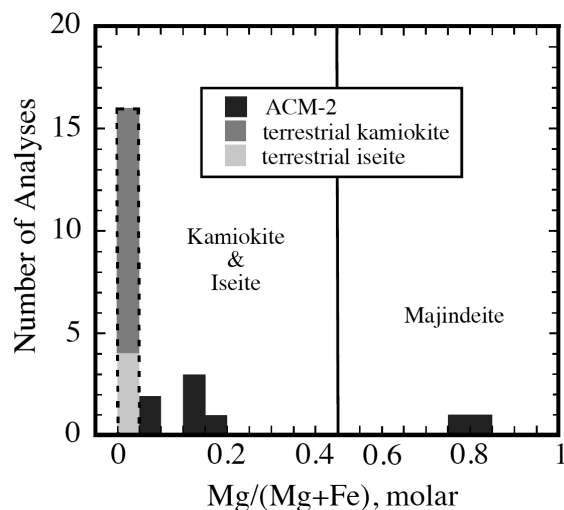


**FIGURE 3.** Histogram of Mg# values of majindeite and kamiokite in *ACM-2*. Mg# values for terrestrial kamiokite and iseite (Sasaki et al. 1985; Johan and Picot 1986; Nishio-Hamane et al. 2013) are indicated as zero on the figure and outlined by dashed lines because MgO contents are not given. As noted in the text, these Mg# values are likely to be very close to zero and, in particular, much lower than in any of the meteoritic phases.

tion suggests that the formation process for majindeite was not driven by access to late-stage, metasomatic, FeO-bearing fluids via spinel. It is also worth noting, in this context, that awaruite is generally present at one end of a kamiokite-bearing assemblage, separating one or more access cracks from magnetite; magnetite is absent from both majindeite occurrences.

Both kamiokite- and majindeite-bearing phase assemblages contain Ni-rich Fe-Ni alloys. Based on EBSD of 8 grains of variable composition (Ni60-82, where Ni<sub>xy</sub> refers to the mole percent of Ni in the alloy) and locality, all of the Fe-Ni alloys in *ACM-2* have an ordered fcc structure (i.e., they are awaruites not taenites). Awaruites associated with majindeite are Ni-rich (Ni74-82) relative to those coexisting with kamiokite (Ni60-68) and overlapping but generally Ni-poor relative to alloy grains in grossular-rich veins (Ni80-86). We observed no correlation between the concentrations of Ni in the alloy or Mg# of kamiokite/majindeite with distance from the rim in *ACM-2*. Alloys in kamiokite- and majindeite-bearing phase assemblages contain inclusions of Ru-,Os-rich alloys. These are not observed in the alloys occurring in grossular-rich veins.

Nb-rich oxides are observed in both kamiokite-(2 of 6) and majindeite-(1 of 2) bearing phase assemblages. We observed apatite in half of the kamiokite-(3 of 6) and majindeite-(1 of 2) bearing phase assemblages. It is possible that all of these assemblages contain apatite but that they are absent in some of our samples due to sectioning effects and/or plucking.

### CRYSTALLOGRAPHY

EBSD analyses at a submicrometer scale were performed on the vibration-polished section USNM 7615 using methods described in Ma and Rossman (2008, 2009a). An HKL (now Oxford) EBSD system on a Zeiss 1550VP scanning electron microscope was used for these measurements and operated at 20 kV and 6 nA in a focused beam configuration with a 70° tilted stage and variable pressure (25 Pa) mode. This approach allows the study of uncoated specimens. The EBSD system was calibrated using a single-crystal silicon standard.

The EBSD pattern for type majindeite from *ACM-2* (Fig. 4a) indicates that the crystal is hexagonal, which means that it cannot correspond to the structure of tugarinovite, which is present elsewhere in the CAI (Ma et al. 2014a), or any of the mixed Mo-oxides (Mg,Fe)MoO<sub>4</sub>, (Mg,Fe)Mo<sub>2</sub>O<sub>7</sub>, or (Mg,Fe)<sub>2</sub>Mo<sub>3</sub>O<sub>12</sub> (Stadnicka et al. 1977; Massarotti et al. 1981; Ehrenberg et al. 1994; Rodriguez et al. 2000; Mikhailik et al. 2008). The structure was determined by matching the observed EBSD pattern (Fig. 4a) with the hexagonal *P6<sub>3</sub>mc* structures of synthetic Mg<sub>2</sub>Mo<sub>3</sub>O<sub>8</sub> (McCarroll et al. 1957; Knorr and Mueller 1995; Abe et al. 2010), and kamiokite (Kanazawa and Sasaki 1986). The best fit (MAD = 0.39) was achieved using the cell parameters of Knorr and Mueller (1995) for Mg<sub>2</sub>Mo<sub>3</sub>O<sub>8</sub>, with *a* = 5.778 Å, *c* = 9.904 Å, *V* = 286.35 Å<sup>3</sup>, and *Z* = 2. Figure 4b shows the EBSD pattern for majindeite from *ACM-2* indexed with the cell parameters for Mg<sub>2</sub>Mo<sub>3</sub>O<sub>8</sub> given by Knorr and Mueller (1995).

Majindeite is isostructural with kamiokite, Fe<sub>2</sub>Mo<sub>3</sub>O<sub>8</sub>, and the Mn-analog iseite (Nishio-Hamane et al. 2013), Mn<sub>2</sub>Mo<sub>3</sub>O<sub>8</sub>. The structure is characterized by alternating Mo-O and Mg-O sheets stacked perpendicular to the hexagonal *c*-axis. Molybdenum is in octahedral coordination with the octahedra forming edge-sharing

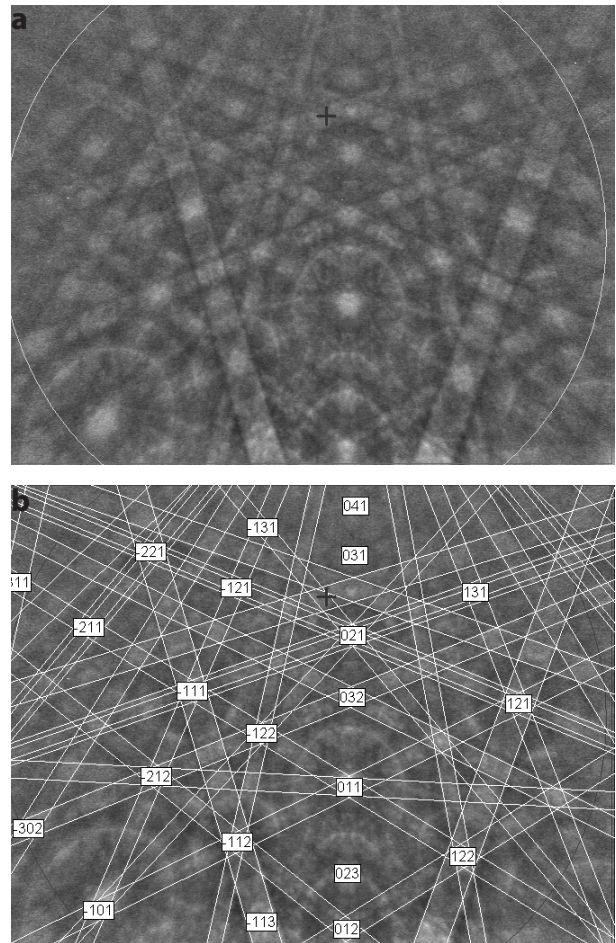


**FIGURE 4.** (a) EBSD pattern of the type majindeite crystal marked with a cross in Figure 1b, and (b) the pattern indexed with the *P6<sub>3</sub>mc* Mg<sub>2</sub>Mo<sub>3</sub>O<sub>8</sub> structure using cell parameters given by Knorr and Mueller (1995).

trimers connected together to form a sheet with hexagonal cavities and unusually short Mo-Mo distances (~2.5 vs. >3.6 Å in other Mo-oxides; e.g., Stadnicka et al. 1977; Massarotti et al. 1981; Kanazawa and Sasaki 1986; Rodriguez et al. 2000). The Mg sheet is composed of vertex-sharing octahedra and tetrahedra that are coordinated to the Mo octahedra of adjacent sheets. The stacking of Mo- and Mg-coordinated sheets leads to a honeycomb structure with cavities aligning parallel to the *c*-axis.

### DISCUSSION

Majindeite is a new member of the kamiokite group of molybdate oxides that assume the nolanite-type *P6<sub>3</sub>mc* structure. This group currently contains kamiokite (Fe<sub>2</sub>Mo<sub>3</sub>O<sub>8</sub>), iseite (Mn<sub>2</sub>Mo<sub>3</sub>O<sub>8</sub>), and majindeite (Mg<sub>2</sub>Mo<sub>3</sub>O<sub>8</sub>), two of which occur in *ACM-2*. Ma et al. (2014a) discuss general constraints on the formation of *ACM-2* and the conditions under which kamiokite formed. Here, we provide a brief overview for the inclusion based on that work and then focus on the origin of majindeite and associated phases.

In *ACM-2*, melilite, spinel, and clinopyroxene, the major ig-

neous phases, crystallized from a partially molten droplet under reducing conditions and formed a classic type B1 CAI roughly 7 mm in diameter with a melilite-rich mantle and a core containing subequal modes of spinel, clinopyroxene, and melilite, and trace to modest amounts of anorthite. The mantle probably crystallized in a partially volatilized region of melt (e.g., Mendybaev et al. 2006; Bullock et al. 2013). The core region of *ACM-2* was later lost, so that the inclusion now consists essentially of a fragment of the melilite-rich mantle with very little of the core material surviving. Within the mantle, alloys and/or alloy-phosphide assemblages containing significant bulk concentrations of Mo  $\pm$  P were incorporated into crystallizing melilite or spinel. In principle, these alloys could have been molten or solid. Peak temperatures for the melting event that produced the melilite-rich mantle probably exceeded the  $\sim 1400$  °C appearance temperature for melilite (e.g., Stolper and Paque 1986; Richter et al. 2006) and, perhaps, the liquidus temperature for the alloy ( $\sim 1440$  °C for the current alloy and somewhat higher if, as is likely, the alloy at this time was more Fe-, Mo-, PGE-enriched than currently; Raghavan et al. 1987). After crystallization of igneous phases, later, low-temperature oxidation/metasomatic event(s) occurred, which led to the introduction of Fe, Na, and, especially, O into the CAI and the partial oxidation of alloys and of phosphides to apatite, the latter requiring mobility of Ca. Kamiokites with Mg# values of 7–20 formed during one of these oxidation events and it is quite probable that majindeite also did so. From a kinetic perspective, majindeite and kamiokite are likely to be favored over other candidate oxides by the unusually small Mo-Mo distances of the structure 2.4 vs.  $>3.6$  Å), especially if a Mo-dominant alloy or phosphide is the phase being oxidized.

We have noted five basic differences, beyond the molybdate composition, between phase assemblages containing majindeite (Mg#  $\sim 80$ ) and those containing kamiokite (Mg# 7–20) in *ACM-2* (Figs. 1–2). (1) The two majindeite-bearing phase assemblages are hosted at least in part by spinel. All of the phase assemblages containing kamiokite (Mg# of 7–20) are hosted by melilite. (2) Majindeite-bearing phase assemblages present smooth interfaces with the host with angles suggesting a crystalline form at the time spinel engulfed the precursor or a negative crystal imposed by host spinel. In contrast, interfaces between kamiokite-bearing assemblages and their host are highly irregular (Fig. 5); also see e.g., Figure 1b of Ma et al. (2014a). (3) The awaruites coexisting with majindeite are more Ni-rich than those coexisting with kamiokite (Ni74–82 vs. Ni60–68). (4) Magnetite is present in outer portions of kamiokite-bearing phase assemblages, separated from major cracks by Fe-Ni alloy, but absent in majindeite-bearing phase assemblages. (5) Both of the host spinels for majindeite are intersected by grossular-rich veins (Figs. 1b and 2b). We observed no grossular-rich veins in the immediate vicinity of kamiokite-bearing phase assemblages. It seems reasonable to expect that compositions of the molybdates are in some way related to one or more of these features and we explore some of the implications below.

The phase assemblage of the inclusion enclosed in spinel (section B2; Fig. 2b) consists of majindeite and alloys with no apatite or phosphide. If the original inclusion consisted only of one or more alloys, then, at the least, a source of Mg (from the spinel or vapor) and oxygen (through a vapor) are required to

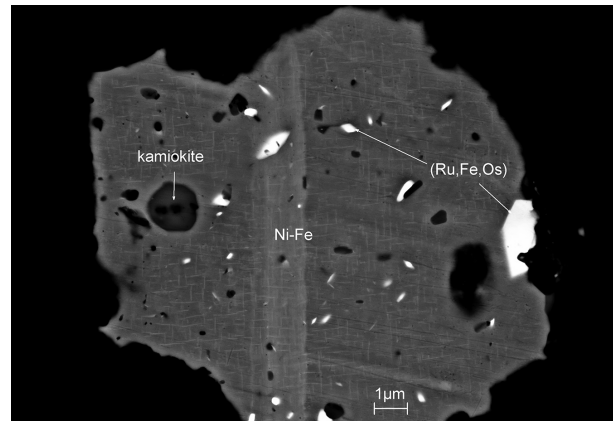
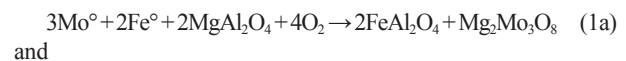


**FIGURE 5.** A kamiokite-bearing phase assemblage within melilite in *ACM-2* (Caltech section Allende 12, section B2). Elongate crystals of Ru-, Os-rich alloys are preferentially aligned along two perpendicular directions; these are usually associated with lower Z shadows within the Ni-Fe alloy matrix, suggesting that the Ru-, Os-alloys preferred Ni, the higher Z element, over Fe. There are also thin ( $\sim 30$  nm thick), cellular-, high-Z lamellae. These are probably not Ni-enriched Fe-Ni alloys because exsolution from awaruite would lead to low Fe-alloys (i.e., darker in BSE); oxidation could lead to Ni-rich lamellae along grain boundaries but the awaruites are single crystals. Note also the highly irregular interface between the phase assemblage and host melilite, which differs in form from Fe-Ni alloys coexisting with majindeite (Figs. 1b and 2b).

produce the observed majindeite. Where apatite is present (e.g., Fig. 1b), Ca mobility is also required, which is consistent with mass-balance calculations suggesting that Ca was lost from CAIs during metasomatism (Wark 1981; Fagan et al. 2013) and the presence of Ca-enriched aureoles in matrix surrounding CAIs (Ford and Brearley 2008). These basic mass-balance considerations lead us to the conclusion that both majindeite and kamiokite formed in systems open to multiple elements.

Type B1 CAIs crystallized under highly reducing conditions, yielding nearly end-member  $MgAl_2O_4$  spinels with Fe in alloy solids or liquids. The initial composition of the alloy, prior to the melting event that produced the mantle of *ACM-2*, would have been a Ni-Fe-Mo-P solid solution with minor Ru, Os, and Ir, possibly with one or more alloys and phosphides that exsolved prior to any oxidation event(s); the most oxidizable element in the alloys would have been Mo, followed by Fe and then Ni [for temperatures below 886 °C, based on Chan et al. (1973) for the Mo-MoO<sub>2</sub> and Fe-wüstite buffers]. Oxidation of alloys/phosphides to oxides and phosphates would have led to significant increases in the total volume of the phase assemblage. The loss of Fe through volatilization may have mitigated some of it; it is likely that volume increases were accommodated through volatilization and cracks.

A simple oxidation mechanism for the formation of majindeite is driven by the reactions



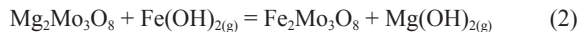
which leads to Fe-bearing majindeite and a Ni-enriched Ni-Fe alloy. However, were Equation 1a to be the governing equilibrium



during the metasomatism associated with Fe enrichment of Mg-Al spinels, we would reasonably expect there to be a connection between the Mg# values of majindeite and host spinel but, based on our sample of two occurrences, this appears not to be the case. The majindeites have essentially the same composition, but the host spinels near majindeite have order of magnitude differences in Fe contents (2 wt% FeO vs. <0.3). We take this to mean that late-stage diffusive Fe-enrichment of spinel was not a significant factor in the formation of majindeite. We view it as much more likely that a fluid was the source of Mg observed in kamiokite and majindeite.

Assuming the phase assemblage of Figure 2b (section B2) to have originated as one or more O-free alloys, we can compute a limiting composition for the original alloy from the current mode and phase compositions. The current mode is ~88 vol% awaruite, 9 vol% majindeite, and 3 vol% Os-Ru-Ir alloy. To convert to a weight and molar basis, we used the density of majindeite from this study and an unweighted linear regression of Tomlinson and Andrews' (1978) data for binary fcc Ni-Fe alloys on the Ni-rich side of the density minimum (i.e., ignoring Pt, which would increase the density). For the Os-Ir-Ru alloy, we assumed solar relative abundances and ideal volumes of mixing and took atomic volumes from Singman (1984). We obtain an "initial" alloy composition of  $\text{Ni}_{68}\text{Fe}_{25}\text{Mo}_2\text{Pt}_1\text{Ru}_1\text{Os}_1\text{Ir}_1$ . The Ni content is at the upper end of the range observed for alloys coexisting with kamiokite (i.e., alloys associated with majindeite and kamiokite may have originally had similar compositions). Note, in this calculation, that the majindeite-bearing phase assemblage is closed with respect to Fe. If a fluid was the source of some (or all) of the Mg, less (or no) Fe from the alloy is required to produce majindeite.

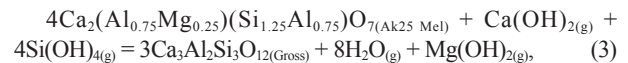
Equation 1a could not be used to constrain environments of formation using our data, even were it pertinent, because concentrations of Mo in the alloys are negligible, reflecting the oxidizing conditions (e.g., Blum et al. 1988). In principle, exchange reactions of the type



could be used for this purpose. However, available thermodynamic data for majindeite and kamiokite in the form of galvanic cell measurements (Rosén and Saitton 1994; Koyama et al. 2003) appear to be inconsistent with each other. For example, the calculated free energy for the reaction  $\frac{1}{2}\text{Mg}_2\text{Mo}_3\text{O}_8 + \text{FeAl}_2\text{O}_4 = \frac{1}{2}\text{Fe}_2\text{Mo}_3\text{O}_8 + \text{MgAl}_2\text{O}_4$  is -489 kJ, referenced to 1000 K. Based on the HSC database, Fe-Mg exchange reactions for  $\text{XAl}_2\text{O}_4$ ,  $\text{XSiO}_3$ ,  $\text{X}_2\text{SiO}_4$ ,  $\text{XMoO}_4$ ,  $\text{X}_2\text{Al}_4\text{Si}_3\text{O}_{18}$ ,  $\text{X}_3\text{Al}_2\text{Si}_3\text{O}_{12}$ , where X refers to Mg and Fe, written in terms of 1 mol each of FeO and MgO should yield free energies in the range of -15 to +26 kJ/mol (e.g., -15 kJ/mol for  $\text{FeO} + \text{MgAl}_2\text{O}_4 = \text{MgO} + \text{FeAl}_2\text{O}_4$ ) and, therefore, equilibria of the type given by spinel-molybdate exchange reaction should not substantially exceed double this range. It therefore seems likely that emfs recorded by at least one of Rosén and Saitton (1994) and Koyama et al. (2003) do not capture their stated reactions.

The association of majindeite occurrences and grossular-rich veins can be used to constrain the environment within which majindeite-bearing phase assemblages were established. Although

metasomatic signatures are pervasive in Allende CAIs, timing and location of alterations are a matter of debate (Krot et al. 1995; Zolensky et al. 2008; MacPherson and Krot 2014 and references therein) and the same is true of majindeite formation. In *ACM-2*, grossular-rich veins typically present collections of grossular grains with sparse spinel; they can have modally significant sodic melilite and rare Ni-rich metal (~Ni80) and a highly aluminous phase (e.g., Fig. 2b). Hydrated phases, which are quite rare in Allende CAIs (e.g., Brearley 2003; Ford and Brearley 2010), dmisteinbergite, monticellite, and Cl-bearing phases, such as wadalite and sodalite, were not observed in *ACM-2*. It is generally thought that the grossular in Allende CAIs resulted directly or indirectly from the breakdown of melilite in the presence of a vapor (e.g., Krot et al. 2007) or as the product of a solid-state reaction between melilite and igneous anorthite (Hutcheon and Newton 1981). In *ACM-2*, grossular-rich veins are in anorthite-free mantle melilite, so the reaction between igneous anorthite and melilite described by Hutcheon and Newton (1981) is not relevant. For Ak25 melilite, typical of melilite shown in Figure 1a, and assuming local conservation of Al in condensed phases, vapor-mediated production of grossular (Gross) alone from melilite (Mel) consumes Ca and Si and releases Mg, for example



where the species  $\text{Ca}(\text{OH})_{2(\text{g})}$ ,  $\text{Mg}(\text{OH})_{2(\text{g})}$ ,  $\text{H}_2\text{O}_{(\text{g})}$ , and  $\text{Si}(\text{OH})_{4(\text{g})}$  in the vapor are chosen because they are the dominant species in oxidized water-rich vapors (e.g., Hashimoto 1992; Plyasunov 2011). If spinel is present, the equilibrium  $4\text{Mel} + 4\text{Si}(\text{OH})_{4(\text{g})} = 2\text{Gross} + 2\text{Ca}(\text{OH})_{2(\text{g})} + \text{Sp}$  also holds. Magnesium is certainly present in the vapor during grossular formation (because it is released by the formation reaction) and this could, in principle, be the source of Mg for the formation of majindeite. If the local vapor was saturated with respect to  $\text{MgAl}_2\text{O}_4$  spinel, which is observed within the adjacent grossular-rich vein, the partial pressure of  $\text{Mg}(\text{OH})_{2(\text{g})}$  could have been locally enhanced relative to values pertinent to the kamiokite-bearing phase assemblages in melilite. For the latter, the ubiquitous presence of magnetite likely buffered molybdates to more Fe-rich compositions. The fact that there are numerous phases containing significant concentrations of Mo (e.g., tugarinovite, molybdenite, kamiokite, majindeite, and Mo-rich magnetite) is a demonstration of the many microenvironments of *ACM-2*.

For kamiokite, grains are often observed as inclusions within alloys and, although these are Fe-rich, as would be expected in the presence of magnetite, they still contain substantial concentrations of Mg, which cannot have been acquired in situ within the alloy. A possible scenario for the formation of these inclusions is that the precursor alloy cracked during metasomatism initiated through grain boundary or lattice diffusion of O with consequent oxidation, thereby providing ready access of vapor to exsolved phosphides and alloys for later alteration. Stress corrosion cracking is a commonly observed phenomenon in Ni-rich steels exposed to  $\text{H}_2\text{O}$ -rich environments (e.g., Capell and Was 2007).

A key issue for understanding the formation of majindeite is the source of oxygen. At the time of crystallization from a melt,

spinel would have been essentially pure  $\text{MgAl}_2\text{O}_4$ , for which bulk transport of oxygen is very slow relative to cation diffusion; self-diffusion of oxygen through  $\text{MgAl}_2\text{O}_4$  is ~4 orders of magnitude slower than for Al, Mg, Fe or of interdiffusion involving cation pairs (Van Orman and Crispin 2010). The same is true of aluminous spinels with solution toward  $\text{Al}_{8/3}\text{O}_4$ , as the excess Al is accommodated through cation and not the oxygen defects that would be needed to significantly speed up bulk transport of oxygen relative to self-diffusion rates (e.g., Ando and Oishi 1974). Nor is the precursor alloy likely to have been a sufficient source of oxygen. The solubility of oxygen can reach weight percent levels in molten alloys (Kjellqvist et al. 2008) and one or more oxides or phosphates may form using this oxygen during cooling, as is sometimes observed in alloys in chondrules from highly unequilibrated ordinary chondrites (e.g., Zanda et al. 1994). However, under the more highly reducing conditions of CAI melting (e.g., Grossman et al. 2008), the solubility of oxygen is negligible. Moreover, this process cannot explain the presence of apatite in the type example (Fig. 1b), which requires the introduction of Ca. Taken together, these considerations lead to the conclusion that the interior of the spinel was open to oxygen and that lattice diffusion of oxygen through the spinel was not important to the oxidation process. This also implies that the inclusions in spinel were open to Ca and Mg. We note that the phase assemblage for one of the majindeite occurrences (Fig. 1b; section USNM 7615) is in contact with a grossular-rich vein. The second occurrence (Fig. 2b; section B2) is completely enclosed by spinel in the plane of the section but there is a grossular-rich vein that is truncated by the spinel. We postulate that the observed inclusion in Figure 2b (section B2) contacted the vein in the third dimension or is at the least, connected to the inclusion through a crack.

Alloy compositions in majindeite-bearing phase assemblages (Ni74-82) overlap the low Ni-end of isolated alloy grains found within grossular-rich veins (Ni80-86) and are distinctly higher than those in contact with kamiokite (Ni60-68). It is also worth noting that a minimalist reconstruction of an initial bulk alloy composition for the majindeite occurrence shown in Figure 2 (section B2) generates a composition (Ni68), consistent with Ni-rich compositions of alloys coexisting with kamiokite and magnetite and with compositions of Ni-Fe alloys coexisting with magnetite in other opaque assemblages in CAIs and chondrules from Allende (e.g., Armstrong et al. 1985; Blum et al. 1988). Because the highest Ni alloys in *ACM-2* coexisting with magnetite is Ni68 and the lowest Ni alloys that do not coexist with magnetite are Ni74, this suggests that there is an oxidation limit near Ni68, whereby alloys more Ni-rich than Ni68 cannot be further oxidized to form magnetite. Such alloys could continue to evolve compositionally through volatilization or sulfidation. At least for *ACM-2*, sulfides appear not to be a major factor because they are not observed in either kamiokite- or majindeite-bearing phase assemblages, and are not common in *ACM-2*; sulfidation was probably not a major process. In terms of volatilization, it is notable that, for alloy compositions in the range of Ni60-86, activity coefficients of Fe and Ni in the alloy are similar (e.g., Swartzendruber et al. 1991) but the equilibrium vapor is highly enriched in Fe relative to Ni based on the HSC database [e.g.,  $\log(P_{\text{Fe}(\text{OH})_2}/P_{\text{Ni}(\text{OH})_2})$  of partial species

$P_i$  in the vapor  $\gg \log(\gamma_{\text{Fe}}/\gamma_{\text{Ni}})$  in the alloy]; thus, volatilization losses of Fe are likely to be much larger than for Ni.

In the above discussion, we outlined the environmental consequences for a suite of observations of kamiokite- and majindeite-bearing phase assemblages. Here, we suggest a scenario by which the observed phase assemblages and their compositions could have been produced. Consider a suite of Ni-Fe-Mo-P alloys with variable Ni/Fe produced during melting and crystallization of the host CAI and incorporated into crystallizing melilite or spinel. This suite of parental alloys may have exsolved phosphides and/or Mo-rich alloys that grew prior to any alteration process but the phase assemblage is dominated by Ni-Fe alloy. The original Ni/Fe ratios are unknown but none of the currently existing kamiokite- or majindeite-bearing phase assemblages appear to have bulk compositions with Ni/Fe low enough to be plausible condensates (e.g., Campbell et al. 2001). These alloy ( $\pm$  phosphide) assemblages were then metasomatized under subsolidus conditions, yielding a net increase of O, Mg, and Ca and a net decrease in Fe.

In Figure 6, we show a cartoon for the evolution of an initial Fe-Ni alloy more Fe-rich than Ni68 with exsolved Mo-rich alloys and phosphides (it is also possible that such phases were produced during the alteration process due to changes in temperature and the composition of the Fe-Ni alloy). We suppose for illustrative purposes that all such Ni-Fe alloys in *ACM-2* were initially more Fe-rich than Ni68 and we ignore Nb oxide, Ru-Os-Ir alloys, monipite, and tugaranovite that are present in some samples. The metasomatizing fluid is oxidizing enough, so that magnetite forms but there is also a net volatilization so that the bulk Fe for the phase assemblage decreases. This phenomenon is at the root of breakaway oxidation of steels (e.g., Pérez-Trujillo and Casteñada 2006; Casteñada and Pérez-Trujillo 2013). If, at the end of the oxidation-volatilization process, magnetite is still present, then the Mo-oxide will be a kamiokite (i.e., Fe-rich). If volatilization proceeds long enough to exhaust the magnetite, kamiokite will then lose Fe (and gain Mg), eventually becoming sufficiently Mg-rich to qualify as a majindeite. Thus, whether or not the molybdate is kamiokite or majindeite turns on whether or not the volatilization process proceeded far enough to exhaust magnetite. Initial alloys for the two majindeite-bearing occurrences were through grossular-rich veins with easy access to external fluids and, we suppose, more extensive reaction than for kamiokite-bearing phase assemblages. In *ACM-2*, magnetites in kamiokite-bearing phase assemblages are invariably concentrated toward one end, separated from major cracks by alloy. This suggests that there was a potential gradient in Fe from a magnetite-saturated alloy at one end to a Ni-rich alloy that interfaced with the vapor at the other. We suggest that two processes were responsible for the observed compositions of alloys and molybdates in *ACM-2*. One was an oxidation reaction of alloy to form magnetite and the second volatilization of the oxide/alloy with net loss of Fe.

## IMPLICATIONS

It is the properties and chemistries of minerals and their petrologic contexts that provide the constraints we have on existing and former environments, whether they be deep within the Earth or nearly lost in time. Mineralogical investigations



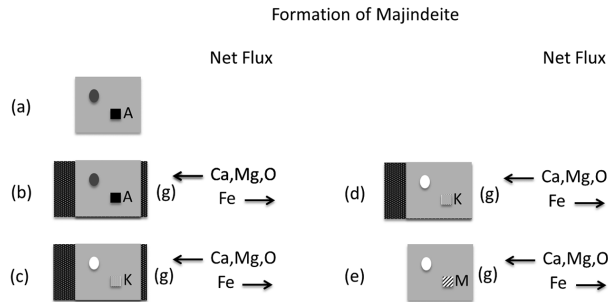


**FIGURE 6.** Cartoon describing the formation of kamiokite and majindeite in *ACM-2*. (a) The initial alloy (light gray) with inclusions of phosphide (medium gray) and Mo-rich alloy (black, labeled “A”). This object is subjected to an oxidizing water-rich gas, leading (b) to the formation of magnetite but with volatilization of Fe into the vapor (i.e., there is a net loss of Fe to the phase assemblage). The Fe-Ni alloy, which is more Fe-rich than Ni68, becomes more Ni-rich through volatilization and oxidation to magnetite. (c) Mo-rich alloy is oxidized to form a Fe-rich, magnetite-saturated kamiokite (stippled, labeled “K”). Phosphides are, at some point oxidized to form apatite. The volatilization process gradually consumes Fe from magnetite and alloy such that the magnetite eventually disappears entirely (d–e). The Fe-Ni alloy at this point is ~Ni68. Subsequent volatilization continues to deplete the alloy in Fe (i.e., the alloy is more Ni-rich than Ni68). The kamiokite is no longer magnetite-saturated, so exchange with the vapor leads to increasing Mg/Fe, ultimately leading to Mg/Fe > 1 and a change in name from kamiokite to majindeite (labeled “M”). Kamiokite-bearing phase assemblages (c–d) are a consequence of Mo-rich alloys oxidized in a magnetite-saturated phase assemblage. Majindeite-bearing phase assemblages (e) are undersaturated with respect to magnetite because the alloy is too Ni-rich.

like the present study address smaller spatial scales than classically considered and these bring new opportunities for better understanding of processes and environments, even for primitive meteorites that have been heavily studied in the past. The studies reveal and characterize new examples of known minerals and micrometer to submicrometer new minerals that can then be interrogated for new information on environment and process. For example, the oxidation of Mo-rich alloys produced majindeite, the topic of this study: this and other newly discovered Mo-oxides in Allende (e.g., tugaranovite, kamiokite) (Ma et al. 2014a), lead to new constraints on post-crystallization oxidation processes after the host Ca-,Al-rich inclusion formed in the early stages of the formation of the Solar System. Recently discovered fine-grained Zr- and Sc-rich phases in Allende and other primitive meteorites (e.g., panguite, kangite, thorveitite, allendeite) speak to vapor-phase condensation in the solar nebula prior to melting or alteration events (i.e., prior to the formation of Ca-,Al-rich inclusions) (Ma et al. 2011a, 2012, 2013, 2014b). Thus, it is not only the new minerals, per se, that are important. Their significance also lies in new statements of environment that complement the questions that can be addressed through other techniques.

#### ACKNOWLEDGMENTS

SEM, EBSD, and EPMA analyses were carried out at the Caltech GPS Division Analytical Facility, which is supported, in part, by NSF Grants EAR-0318518 and DMR-0080065. J.R.B. acknowledges NASA grant NNG04GG14G. We thank Steven Simon, Makoto Kimura, and associate editor Rhian Jones for their constructive reviews.

#### REFERENCES CITED

- Abe, H., Sato, A., Tsujii, N., Furubayashi, T., and Shimoda, M. (2010) Structural refinement of  $T_2Mo_3O_8$  ( $T = Mg, Co, Zn$  and Mn) and anomalous valence of trinuclear molybdenum clusters in  $Mn_2Mo_3O_8$ . *Journal of Solid State Chemistry*, 183, 379–384.
- Ando, K., and Oishi, Y. (1974) Self-diffusion coefficients of oxygen ion in single crystals of  $MgO \cdot nAl_2O_3$  spinels. *Journal of Chemical Physics*, 61, 625–629.
- Armstrong, J.T. (1995) CITZAF: a package of correction programs for the quantitative electron microbeam X-ray analysis of thick polished materials, thin films, and particles. *Microbeam Analysis*, 4, 177–200.
- Armstrong, J.T., El Goresy, A., and Wasserburg, G.J. (1985) Willy: A noble Ur-Fremdling—Its history and implications for the formation of Fremdlinge and CAI. *Geochimica et Cosmochimica Acta*, 49, 1001–1022.
- Beckett, J.R., and Grossman, L. (1988) The origin of type C inclusions from carbonaceous chondrites. *Earth and Planetary Science Letters*, 89, 1–14.
- Blum, J.D., Wasserburg, G.J., Hutcheon, I.D., Beckett, J.R., and Stolper, E.M. (1988) Origin of opaque assemblages in C3V meteorites: Implications for nebular and planetary processes. *Geochimica et Cosmochimica Acta*, 53, 543–556.
- Brearley, A.J. (2003) Nebular versus parent-body processing. In A.M. Davis, Ed., *Treatise on Geochemistry*, 1, p. 247–268. Elsevier, Amsterdam.
- Bullock, E.S., Knight, K.B., Richter, F.M., Kita, N.T., Ushikubo, T., MacPherson, G.J., Davis, A.M., and Mendybaev, R.A. (2013) Mg and Si isotopic fractionation patterns in types B1 and B2 CAIs: Implications for formation under different nebular conditions. *Meteoritics & Planetary Science*, 48, 1440–1458.
- Campbell, A.J., Humayun, M., Meibom, A., Krot, A.N., and Keil, K. (2001) Origin of zoned metal grains in the QUE94411 chondrite. *Geochimica et Cosmochimica Acta*, 65, 163–180.
- Capell, B.M., and Was, G.S. (2007) Selective internal oxidation as a mechanism for intergranular stress corrosion cracking of Ni-Cr-Fe alloys. *Metallurgical and Materials Transactions*, 38A, 1244–1259.
- Castañeda, S.I., and Pérez-Trujillo, F.J. (2013) Microstructure and volatile species determination of ferritic/martensitic FB2 steel in contact with Ar + 40 %  $H_2O$  at high temperatures. *Oxidation of Metals*, 79, 147–166.
- Chan, J.C., Alcock, C.B., and Jacob, K.T. (1973) Electrochemical measurement of the oxygen potential of the system iron-alumina-hercynite in the temperature range 750 to 1600°C. *Canadian Metallurgical Quarterly*, 12, 439–443.
- Clarke, R.S., Jarosewich, E., Mason, B., Nelen, J., Gomez, M., and Hyde, J.R. (1971) The Allende, Mexico, meteorite shower. *Smithsonian Contributions to the Earth Science*, 5, 1–53.
- Ehrenberg, H., Wltschek, G., Kroener, T., Weitzel, H., and Fuess, H. (1994) Magnetic structures of  $\alpha$ - $FeMoO_4$  and  $\alpha$ - $CoMoO_4$ . *Journal of Magnetism and Magnetic Materials*, 135, 355–360.
- Fagan, T.J., Washio, M., and Aragane, H. (2013) Open-system behavior during formation of grossular-rich veins in Allende CAIs. *Meteoritics & Planetary Science*, 48(S1), A116.
- Ford, R.L., and Brearley, A.J. (2008) Element exchange between matrix and CAIs in the Allende meteorite. 39th Lunar and Planetary Science Conference Abstract 2399.
- (2010) Discovery of vesuvianite and kaolinite formed during the alteration of melilite in an Allende type A CAI: Characterization by FIB/TEM. 41st Lunar and Planetary Science Conference, Abstract 1402.
- Grossman, L., Ebel, D.S., Simon, S.B., Davis, A.M., Richter, F.M., and Parsad, N.M. (2000) Major element chemical and isotopic compositions of refractory inclusions in C3 chondrites: The separate roles of condensation and evaporation. *Geochimica et Cosmochimica Acta*, 64, 2879–2894.
- Grossman, L., Beckett, J.R., Fedkin, A.V., Simon, S.B., and Ciesla, F.J. (2008) Redox conditions in the solar nebula: Observational, experimental, and theoretical constraints. *Reviews in Mineralogy and Geochemistry*, 68, 93–140.
- Hashimoto, A. (1992) The effect of  $H_2O$  gas on volatilities of planet-forming major elements: I. Experimental determination of thermodynamic properties of Ca-, Al-, and Si-hydroxide gas molecules and its application to the solar nebula. *Geochimica et Cosmochimica Acta*, 56, 511–532.
- Hutcheon, I.D., and Newton, R.C. (1981) Mg isotopes, mineralogy, and mode of formation of secondary phases in C3 refractory inclusions. *Lunar Science Conference*, 12, 491–493.
- Johan, Z., and Picot, P. (1986) Kamiokite,  $Fe_2Mo_3O_8$ , a tetravalent molybdenum oxide: New data and occurrences. *Tschermak's Mineralogische und Petrographische Mitteilungen*, 35, 67–75.
- Kanazawa, Y., and Sasaki, A. (1986) Structure of kamiokite. *Acta Crystallographica*, C42, 9–11.
- Kjellqvist, L., Selleby, M., and Sundman, B. (2008) Thermodynamic modelling of the Cr-Fe-Ni-O system. *Calphad*, 32, 577–592.
- Knor, R., and Mueller, U. (1995)  $\eta$ - $Mo_2O_{11}$  und  $Mg_2Mo_3O_8$ : eine neue Synthese und Verfeinerung ihrer Kristallstrukturen. *Zeitschrift für anorganische und allgemeine Chemie*, 621, 541–545.
- Koyama, K., Morishita, M., Harada, T., and Maekawa, N. (2003) Determination of standard Gibbs energies of formation of  $Fe_2Mo_3O_{12}$ ,  $Fe_2Mo_3O_8$ ,  $Fe_2MoO_4$ , and  $FeMoO_4$  of the Fe-Mo-O ternary system and  $\mu$  phase of the Fe-Mo binary system by electromotive force measurement using a  $Y_2O_3$ -stabilized  $ZrO_2$  solid

- electrolyte. *Metallurgical Transactions B*, 34B, 653–659.
- Krot, A.N., Scott, E.R.D., and Zolensky, M.M. (1995) Mineralogical and chemical modification of components in CV3 chondrites: Nebular or asteroidal? *Meteoritics*, 30, 748–775.
- Krot, A.N., Yurimoto, H., Hutcheon, I.D., Libourel, G., Chaussidon, M., Tissandier, L., Petaev, M.I., MacPherson, G.J., Paque-Heather, J., and Wark, D. (2007) Type C Ca, Al-rich inclusions from Allende: Evidence for multistage formation. *Geochimica et Cosmochimica Acta*, 71, 4342–4364.
- Ma, C. (2013) Majindeite, IMA 2012-079. *CNMNC Newsletter No. 15*, February 2013, page 10. *Mineralogical Magazine*, 77, 1–12.
- (2015a) Discovery of nuwaite,  $\text{Ni}_3\text{GeS}_2$ , a new alteration mineral in Allende. *Meteoritics and Planetary Science*, 50 (S1), A5151.
- (2015b) Nanomineralogy of meteorites by advanced electron microscopy: Discovering new minerals and new materials from the early solar system. *Microscopy and Microanalysis*, 21 (Suppl. 3), 2353–2354. DOI:10.1017/S1431927615012544.
- Ma, C., and Rossman, G.R. (2008) Barioperovskite,  $\text{BaTiO}_3$ , a new mineral from the Benitoite Mine, California. *American Mineralogist*, 93, 154–157.
- (2009a) Tistarite,  $\text{Ti}_2\text{O}_3$ , a new refractory mineral from the Allende meteorite. *American Mineralogist*, 94, 841–844.
- (2009b) Grossmanite,  $\text{CaTi}^{3+}\text{AlSiO}_6$ , a new pyroxene from the Allende meteorite. *American Mineralogist*, 94, 1491–1494.
- Ma, C., Beckett, J.R., and Rossman, G.R. (2009) Discovery of a Mg-dominant analog of karniokite,  $\text{Mg}_2\text{Mo}_3\text{O}_8$ , a new mineral from an Allende Type B1 CAI. *Meteoritics & Planetary Science*, 44 (S), A128.
- Ma, C., Beckett, J.R., Tschauner, O., and Rossman, G.R. (2011a) Thortveitite ( $\text{Sc}_2\text{Si}_2\text{O}_7$ ), the first solar silicate? *Meteoritics & Planetary Science*, 46, A144.
- Ma, C., Kampf, A.R., Connolly, H.C., Beckett, J.R., Rossman, G.R., Sweeney Smith, S.A., and Schrader, D.L. (2011b) Krotite,  $\text{CaAl}_2\text{O}_4$ , a new refractory mineral from the NWA 1934 meteorite. *American Mineralogist*, 96, 709–715.
- Ma, C., Tschauner, O., Beckett, J.R., Rossman, G.R., and Liu, W. (2012) Panguite,  $(\text{Ti}^{4+}, \text{Sc}, \text{Al}, \text{Mg}, \text{Zr}, \text{Ca})_{18}\text{O}_{30}$ , a new ultra-refractory titania mineral from the Allende meteorite: Synchrotron micro-diffraction and EBSD. *American Mineralogist*, 97, 1219–1225.
- Ma, C., Tschauner, O., Beckett, J.R., Rossman, G.R., and Liu, W. (2013) Kangite,  $(\text{Sc}, \text{Ti}, \text{Al}, \text{Zr}, \text{Mg}, \text{Ca}, \square)_2\text{O}_3$ , a new ultrarefractory scandia mineral from the Allende meteorite: Synchrotron micro-Laue diffraction and electron backscatter diffraction. *American Mineralogist*, 98, 870–878.
- Ma, C., Beckett, J.R., and Rossman, G.R. (2014a) Monipite,  $\text{MoNiP}$ , a new phosphide mineral in a Ca-Al-rich inclusion from the Allende meteorite. *American Mineralogist*, 99, 198–205.
- (2014b) Allendeite ( $\text{Sc}_2\text{Zr}_2\text{O}_{12}$ ) and hexamolybdenum ( $\text{Mo}, \text{Ru}, \text{Fe}$ ), two new minerals from an ultrarefractory inclusion from the Allende meteorite. *American Mineralogist*, 99, 654–666.
- Ma, C., Paque, J., and Tschauner, O. (2015) Beckettite, IMA 2015-001. *CNMNC Newsletter No. 25*, June 2015, page 531. *Mineralogical Magazine*, 79, 529–535.
- MacPherson, G.J., and Krot, A.N. (2014) The formation of Ca-, Fe-rich silicates in reduced and oxidized CV chondrites: The roles of impact-modified porosity and permeability, and heterogeneous distribution of water ices. *Meteoritics & Planetary Science*, 49, 1250–1270.
- Massarotti, V., Flor, G., and Marini, A. (1981) Crystal data for ferric molybdate:  $\text{Fe}_2(\text{MoO}_4)_3$ . *Journal of Applied Crystallography*, 14, 64–65.
- McCarroll, W.H., Katz, L., and Ward, R. (1957) Some ternary oxides of tetravalent molybdenum. *Journal of the American Chemical Society*, 79, 5410–5414.
- Mendybaev, R.A., Davis, A.M., and Richter, F.M. (2006) Crystallization of melilite from CMAS-liquids and the formation of the melilite mantle of type B1 CAIs: Experimental simulations. *Geochimica et Cosmochimica Acta*, 70, 2622–2642.
- Mikhailik, V.B., Kraus, H., Kapustyanyk, V., Panasyuk, M., Prots, Yu., Tsybul'skiy, V., and Vasylychko, L. (2008) Structure, luminescence and scintillation properties of the  $\text{MgWO}_4\text{-MgMo}_4$  system. *Journal of Physics: Condensed Matter*, 20, 365219, 8 pp.
- Nakayama, S., Nakamura, R., Akaki, M., Akahoshi, D., and Kuwahara, H. (2011) Ferromagnetic behavior of  $(\text{Fe}_{1-y}\text{Zn}_y)_2\text{Mo}_3\text{O}_8$  ( $0 \leq y \leq 1$ ) induced by nonmagnetic Zn substitution. *Journal of the Physical Society of Japan*, 80, 104706, 4 pp.
- Nishio-Hamane, D., Tomita, N., Minakawa, T., and Inaba, S. (2013) Iseite,  $\text{Mn}_2\text{Mo}_3\text{O}_8$ , a new mineral from Ise, Mie prefecture, Japan. *Journal of Mineralogical and Petrological Sciences*, 108, 37–41.
- Paque, J.M., Beckett, J.R., Ishii, H.A., Aléon-Toppiani, A., Burnett, D.S., Teslich, N., Dai, Z.R., and Bradley, J.P. (2009) The formation of boundary clinopyroxenes and associated glass veins in type B1 CAIs. *Meteoritics & Planetary Science*, 44, 665–687.
- Pérez-Trujillo, F.J., and Casteñada, S.I. (2006) Study by means of the mass spectrometry of volatile species in the oxidation of Cr,  $\text{Cr}_2\text{O}_3$ , Al,  $\text{Al}_2\text{O}_3$ , Si,  $\text{SiO}_2$ , Fe and ferritic/martensitic steel samples at 923 K in Ar + (10 to 80%) $\text{H}_2\text{O}$  vapor atmosphere for new-materials design. *Oxidation of Metals*, 66, 231–251.
- Plyasunov, A.V. (2011) Thermodynamic properties of  $\text{H}_4\text{SiO}_4$  in the ideal gas state as evaluated from experimental data. *Geochimica et Cosmochimica Acta*, 75, 3853–3865.
- Pouchou, J.-L., and Pichoir, F. (1991) Quantitative analysis of homogeneous or stratified microvolumes applying the model “PAP”. In K.F.J. Heinrich and D.E. Newbury, Eds., *Electron Probe Quantitation*, p. 31–75. Plenum Press, New York.
- Raghavan, V., Raynor, G.V., and Rivlin, V.G. (1987) Phase Diagrams of Ternary Iron Alloys: Phase Equilibria in Iron Ternary Alloys. ASM International, Ann Arbor, Michigan, 485 pp.
- Richter, F.M., Mendybaev, R.A., and Davis, A.M. (2006) Conditions in the protoplanetary disk as seen by the type B CAIs. *Meteoritics & Planetary Science*, 41, 83–93.
- Rodríguez, J.A., Hanson, J.C., Chaturvedi, S., Maiti, A., and Brito, J.L. (2000) Studies on the behavior of mixed-metal oxides: structural, electronic, and chemical properties of  $\beta\text{-FeMoO}_4$ . *Journal of Physical Chemistry B*, 104, 8145–8152.
- Rosén, E., and Saitton, B. (1994) Studies of phase equilibria in the system Mg-Mo-O in the temperature range 1100–1400 K. *Acta Chemica Scandinavica*, 48, 720–723.
- Sasaki, A., Yui, S., and Yamaguchi, M. (1985) Kamiokite,  $\text{Fe}_2\text{Mo}_3\text{O}_8$ , a new mineral. *Mineralogical Journal*, 12, 393–399.
- Singman, C.N. (1984) Atomic volume and allotropy of the elements. *Journal of Chemical Education*, 61, 137–142.
- Stadnicka, K., Haber, J., and Kozłowski, R. (1977) The crystal structure of magnesium dimolybdate. *Acta Crystallographica*, B33, 3859–3862.
- Stolper, E., and Paque, J.M. (1986) Crystallization sequences of Ca-Al-rich inclusions from Allende: The effects of cooling rate and maximum temperature. *Geochimica et Cosmochimica Acta*, 50, 1785–1806.
- Swartzendruber, L.J., Itkin, V.P., and Alcock, C.B. (1991) The Fe-Ni (iron-nickel) system. *Journal of Phase Equilibria*, 12, 288–312.
- Tomlinson, W.J., and Andrews, A.J. (1978) Densities of fcc nickel-iron alloys. *Metal Science*, 12, 263–264.
- Van Orman, J.A., and Crispin, K.L. (2010) Diffusion in oxides. *Reviews in Mineralogy and Geochemistry*, 72, 757–825.
- Wark, D.A. (1981) The pre-alteration compositions of Allende Ca-Al condensates. *Lunar and Planetary Science*, 12, 1148–1150.
- Zanda, B., Bourot-Denise, M., Perron, C., and Hewins, R.H. (1994) Origin and metamorphic redistribution of silicon, chromium, and phosphorus in the metal of chondrites. *Science*, 265, 1846–1849.
- Zolensky, M.E., Krot, A.N., and Benedix, G. (2008) Record of low-temperature alteration in asteroids. *Reviews in Mineralogy and Geochemistry*, 68, 429–462.

MANUSCRIPT RECEIVED MAY 4, 2015

MANUSCRIPT ACCEPTED DECEMBER 24, 2015

MANUSCRIPT HANDLED BY RHIAN JONES